IONOSPHERIC LONGITUDINAL VARIABILITY IN THE NORTHERN HEMISPHERE DURING MAGNETIC STORMS IN MARCH 2012 FROM IONOSONDE AND GPS/GLONASS DATA

M.A. Chernigovskaya (iD)
Institute of Solar-Terrestrial Physics SB RAS,
Irkutsk, Russia, cher@iszf.irk.ru

A.S. Yasyukevich (iD)
Institute of Solar-Terrestrial Physics SB RAS,
Irkutsk, Russia, annpol@iszf.irk.ru

D.S. Khabituev (iD)
Institute of Solar-Terrestrial Physics SB RAS,
Irkutsk, Russia, khabituev@iszf.irk.ru

Abstract. A comprehensive study of spatio-temporal variations of geomagnetic, ionospheric, and atmospheric parameters in the middle and high latitudes of the Northern Hemisphere during a series of magnetic storms in March 2012 has been expanded by including vertical total electronic content (TEC) data from measurements at the chains of dual-frequency phase receivers GPS/GLONASS in the analysis. The features of longitudinal variations in ionosphere ionization over mid-latitude Eurasia, found earlier from vertical sounding data, are confirmed by vertical TEC data. We emphasize the complex physics of the long magnetically disturbed period in March 2012 with switching between positive and negative effects of an ionospheric storm during the same magnetic storm phases for spaced mid-latitude regions of the Eastern Hemisphere. Such changes in the ionospheric storm effects might have been caused by the superposition of competing processes in the mid-latitude region of the Eastern Hemisphere due to variations in the thermospheric composition, thermospheric winds, and large-scale electric fields affecting ionospheric ionization. We have observed significant differences in the nature of the ionospheric ionization reaction between the Eastern and Western hemispheres to the prolonged geomagnetic disturbance in March 2012. According to TEC data, there was an effect of reduced ionization of the ionosphere at longitudes of the Western Hemisphere, unlike the Eastern one. The effect of a negative ionospheric storm was caused by the formation of vast areas of atmospheric gas with a reduced density ratio $[O]/[N_2]$ over the mid-latitude region of the Western Hemisphere in the zone of maximum penetration of geomagnetic disturbances from high latitudes to middle latitudes. According to the INTERMAGNET magnetometer chain data for the analyzed period of magnetic storms on March 7–20, 2012, at midlatitudes of the Northern Hemisphere the maximum geomagnetic field variations were observed in the Western Hemisphere.

Keywords: chain of GPS/GLONASS receivers, ionosonde chain, ionospheric and thermospheric disturbances, geomagnetic field variations, geomagnetic storm.

INTRODUCTION

The purpose of this paper is to study the spatio-temporal variations of parameters in the magnetosphere—ionosphere—thermosphere system during periods of increased solar activity (solar flares, coronal mass ejections, high-speed streams from coronal holes) when there is a sharp increase in the solar wind velocity for extended periods (from several to many hours). The interaction of the high-energy solar wind with the main geomagnetic field (GMF) leads to significant perturbations in the GMF strength, which are called geomagnetic storms [Dudok de Wit, Watermann, 2009].

During magnetic storms, a whole complex of processes develop in the ionosphere (ionospheric storms), which cause its parameters to change considerably [Prölss, 1995; Rishbeth, 1998; Buonsanto, 1999]. Disturbances in Earth's ionosphere are primarily generated by a sequence of interrelated events that begin with manifestations of increased solar activity, which then alter the solar wind—magnetosphere—ionosphere system. In other cases, ionospheric disturbances are triggered by internal factors in the ionosphere—thermosphere system, which are associated with processes in a neutral atmosphere. Ionospheric ionization disturbances of different intensity and different spatial and temporal scales occur in both cases.

Ionospheric storms are accompanied by significant variations in the F2-layer critical frequency f_oF2, which is proportional to the F-region peak electron density [Polyakov et al., 1968]. During geomagnetic disturbances, f_oF2 may decrease or increase in comparison with the values under quiet conditions (negative or positive ionospheric storms respectively) [Matsushita, 1959]. Perturbed electric fields generated during magnetic storms [Tsurutani et al., 2004; Huang, 2013] — 1) almost instantly appearing prompt penetration electric fields (PPEFs) often observed in equatorial latitudes, and 2) electric fields with a delay created by a perturbed dynamo as a result of Joule heating due to energy input during a magnetic storm at high latitudes — can cause large upwelling or downwelling ionospheric plasma

streams leading to large-scale increases or decreases in ionization and vertical total electron content (TEC). Development of negative and positive effects of ionospheric storms strongly depends on local time, season, and geographic region [Prölss, 1995; Rishbeth, 1998; Buonsanto, 1999; Mendillo, 2006; Burešová et al., 2007].

Negative ionospheric storms are the dominant characteristic in the ionospheric response to enhanced geomagnetic activity and are generally associated with an equatorward shift of the main ionospheric trough [Prölss, 1995; Rishbeth, 1998]. Seaton [1956] was the first to suggest that a decrease in electron density may be caused by variations in the thermospheric neutral gas composition. Enhancement of the westward auroral electrojet at high latitudes induces neutral winds, which redistribute the neutral atmospheric composition over most of the high-latitude region and part of the midlatitude region. Above the turbopause (about 120 km), the diffusion separation of atmospheric gases begins. The higher, the greater the amount of oxygen is in the atomic state. At altitudes 200–300 km and above, atomic oxygen, which, as a lighter gas, is transferred more intensively than molecular nitrogen, becomes predominant. This, in turn, leads to a decrease in $[O]/[N_2]$ in the upper atmosphere and hence to negative perturbations of the electron density in the ionospheric F-region [Mayr, Volland, 1972; Laštovička, 2002; Prölss, Werner, 2002; Danilov, 2003; Liou et al., 2005; Klimenko et al., 2011].

Positive ionospheric storms are caused by an increase in equatorward neutral winds occurring due to energy input into auroral latitudes during a magnetic storm [Prölss, 1995]. When positive ionospheric storms occur, the effects of neutral winds prevail over changes in the chemical composition in midlatitudes. Another cause for the positive ionospheric storm effects is the processes in the equatorial latitudes during geomagnetic storms. PPEFs intensify the electrodynamic drift $\vec{E} \times \vec{B}$ near the equator, causing ionospheric plasma to rise up to 800–1000 km [Astafyeva, 2009]. A giant plasma fountain (Dayside Ionospheric Superfountain) is formed, transporting plasma from the equatorial region to higher altitudes and higher latitudes [Tsurutani et al., 2004]. According to Danilov [2013], PPEFs responsible for the positive effects of ionospheric storms, which occur in low and mid-low latitudes even during moderate storms, mask the negative ionospheric storm effects. Photoionization of the lower *F*-region produces a "new" plasma, which compensates for the plasma raised up by the drift $\vec{E} \times \vec{B}$, thereby bringing about an increase in TEC. This is the dominant effect of positive ionospheric storms in midlatitudes.

Thus, processes in a neutral atmosphere are an essential part of the complex sequence of electrodynamic and chemical processes developing in the ionosphere—thermosphere system during periods of heliogeomagnetic activity. Satellite data on atmospheric composition variations in the thermosphere is often used to study relationships between these processes. In particular, the Global Ultraviolet Imager (GUVI) aboard the NASA TIMED satellite [Christensen et al., 2003] is employed to measure $[O]/[N_2]$ in a column of thermospheric gas

above 100 km. This physical parameter is one of the key parameters determining the state of the ionosphere—thermosphere system during ionospheric storms. It reflects the circulation of atomic oxygen in the thermosphere and is a good indicator for negative phases of ionospheric storms.

At the previous stages of the research based on data from the Eurasian mid-latitude ionosonde chain, as well as mid- and high-latitude chains of GPS/GLONASS receivers and INTERMAGNET magnetometers, longitude features of the ionospheric response to extreme magnetic storms in March and June 2015 [Shpynev et al., 2018; Chernigovskaya et al., 2019, 2020; Chernigovskaya et al., 2021a] and to a strong magnetic storm in October 2016 [Chernigovskaya et al., 2021b] were analyzed. Chernigovskaya et al. [2022a, b] continued to examine ionospheric effects of magnetic storms, using a proven method of analyzing geomagnetic and ionospheric ionosonde data for a series of magnetic storms in March 2012.

The in-depth analysis carried out earlier has allowed us to conclude that the main cause for the longitude variations in ionospheric parameters is the longitude features of the main GMF structure and its variations when geomagnetic conditions change, as well as the mismatch between the magnetic and geographic poles (the so-called UT variations).

Low ionization values during the storm recovery phase (2–4 days after the main phase) may be due to westward propagation of an atmospheric wave of neutral gas with low $[O]/[N_2]$ over midlatitudes. This wave is formed in the lower thermosphere of polar latitudes in the nightside sector with a strong westward electrojet flowing during the magnetic storm main phase. Due to the high frequency of collisions between molecular ions and neutrals, such a wave acquires a large scale and momentum and moves over long distances even though the ionospheric source is "switched off" in auroral latitudes.

In this paper, we continue and expand the study of the above physical mechanisms by including measurement data obtained from chains of GPS/GLONASS dual-frequency phase receivers during a series of magnetic storms in March 2012 in analysis [Chernigovskaya et al., 2022a, b].

EXPERIMENTAL MEASUREMENT DATA

To analyze spatio-temporal variations in ionospheric parameters during a long geomagnetic disturbance in March 2012, we have used 1) TEC measurement data from mid- and high-latitude chains of GPS/GLONASS dual-frequency phase receivers (Figure 1, *a*); 2) measurement data on hourly average F2-layer critical frequency f_oF2 from the chain of seven mid-latitude ionosondes, located in a latitude range ~50°–60° N spaced 15°–20° apart in longitude in the 13°–158° E sector of the Eurasian continent (Figure 1, *b*); 3) measurement data on variations in the GMF *H* and *Z* components from mid- and high-latitude chains of INTERMAGNET magnetometers [http://www.intermagnet.org] (Figure 1, *b*); 4) satellite measurements of $[O]/[N_2]$ in a column of
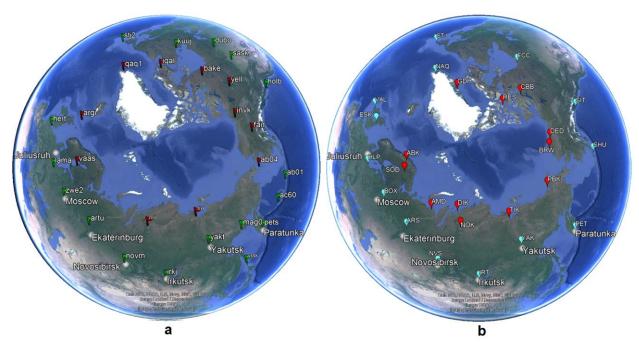
Figure 1. Location of chains of ionosondes and GPS/GLONASS receivers (*a*); ionosondes and magnetometers (*b*)

atmospheric gas in the thermosphere (ionosphere) above ~100 km, performed by an optical method with the TIMED/GUVI spectrograph [http://guvitimed.jhuapl.edu/guvi-galleryl3on2].

The mid-latitude chain consists of 15 GPS/GLONASS receivers in a latitude range 50°–55° N (panel *a*, green flags). The high-latitude chain contains 13 GPS/GLONASS receivers in a latitude range 65°–70° N (panel *a*, red flags). Detailed information about the stations that make up the GPS/GLONASS receiver chains can be found in [Chernigovskaya et al., 2020; Chernigovskaya et al., 2021a). Vertical TEC has been calculated from initial data sets by the model of absolute TEC, taking into account differential code delays [Yasyukevich et al., 2015].

The Eurasian mid-latitude ionosonde chain (panel *b*, white circles) included the ionosonde AIS (Paratunka), two Russian ionosondes Parus of different modifications (Novosibirsk, Ekaterinburg), and four DPS-4 digital ionosondes of different modifications (Yakutsk, Irkutsk, Moscow, Juliusruh). A detailed description of the ionosondes, as well as the method of processing and analyzing the ionospheric parameters (critical frequency and height of F2-layer maximum ionization), can be found in [Chernigovskaya et al., 2021a; Chernigovskaya et al., 2022a]. The papers also describe the mid- and high-latitude chains of INTERMAGNET magnetometers (panel *b*) and the method of analyzing variations in the GMF *H* and *Z* components.

ANALYSIS
OF HELIOGEOMAGNETIC
CONDITIONS
AND GMF VARIATIONS

The period of enhanced geomagnetic activity we analyze in this paper includes a series of four magnetic storms on March 7, 9, 12, and 15, 2012 (S1–S4, Table). Development of the heliogeomagnetic events is described in detail by Chernigovskaya et al. [2022a]. Solar activity was high on March 5–7, 9–10, and 13–14 mainly due to a series of long large solar flares X1.1 (March 5), X5.4 (March 7), M6.3 (March 9), M8.4 (March 10), M7.9 (March 13), M2.8 (March 14) from active region 1429 [Tsurutani et al., 2014]. All the flares were connected with earthward coronal mass ejections (CMEs). During the period of interest, a high-speed stream from one coronal hole (CH HSS — coronal hole high-speed stream) occurred. It lasted from March 16 to March 18 after sudden commencement of magnetic storm S4 (sudden storm commencement (SSC)). It is well known that CH HSS events also cause geomagnetic activity to increase. All the four magnetic storms are associated with increased solar wind velocities related to CMEs and CH HSS, higher intensity of the interplanetary magnetic field, plasma density and temperature.

To analyze the GMF variability during the magnetic storms in March 2012, we use the standard deviation of the GMF *H* and *Z* components relative to the background undisturbed values. Figure 2 shows longitude-time distributions of standard deviations of the GMF *H* and *Z* components in the Northern Hemisphere, obtained by INTERMAGNET magnetometer chains at middle (panel *a*) and high (panel *b*) latitudes.

In the longitude distribution of GMF variations, as in our previous studies of magnetic storms occurring in 2015 and 2016 [Shpynev et al., 2018; Chernigovskaya et al., 2019, 2020, 2021b; Chernigovskaya et al., 2021a], particularly noticeable are the longitudes at which the intensity of the variations has maxima and minima. Maximum variability in the standard deviations of the GMF *H* and *Z* components is generally observed at midlatitudes (near ~55° N) (panel *a*). At high latitudes

Characteristics of geomagnetic storms in March 2012

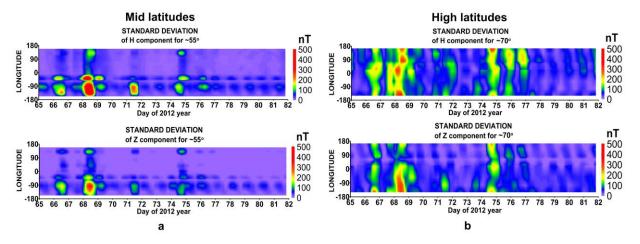| Storm number	Parameters at a maximum of the geomagnetic storm [http://wd c.kugi.kyoto-u.ac.jp]			Storm intensity	
	Dst index (Figure 3, *c*, *d*)	K_p index	A_p index	According to the *Dst* index [Loewe, Prölss, 1997]	According to NASA's classification [https://www.swpc.noaa.gov/noaa-scales-explanation]
S1	−85 nT at 15:00 UT on March 07, 2012	6$_o$	80 nT	moderate	Class G2
S2	−143 nT at 08:00 UT on March 09, 2012	8$_o$	207 nT	strong	Class G4
S3	−51 nT at 16:00 UT on March 12, 2012	6$_+$	94 nT	moderate	Class G2
S4	−80 nT at 19:00 UT on March 15, 2012	6$_+$	94 nT	moderate	Class G2

Figure 2. Longitude-time variations of standard deviations of the GMF *H* and *Z* components on March 6–22, 2012 (UT) in middle ~55° N (*a*) and high ~70° N (*b*) latitudes

(near ~70° N), GMF variability is more uniform in longitude (panel *b*), but longitude irregularities of GMF variations are also manifested. We believe that the irregular structure of longitude variability in the GMF components stems from spatial anomalies of different scales in the main geomagnetic field, as well as from the mismatch between the magnetic and geographic poles (UT effect).

During the March 7–20, 2012 magnetic storms we analyze, in the mid-latitude region of the Northern Hemisphere maximum variations in the GMF components were recorded in the Western Hemisphere in the direction of the meridian of the geomagnetic pole near ~90° W and at longitudes of ~45° W and ~135° W (see Figure 2, *a*). In the midlatitudes of the Eastern Hemisphere, GMF variability was significantly lower. A zone of higher GMF variations appeared in ~120–140° N longitudes over the Far East of Eurasia.

The longitudes, where strong variations in the GMF strength are observed, correspond to the zones of maximum penetration of geomagnetic disturbances from high latitudes to middle latitudes. These regions feature strong negative ionospheric ionization disturbances, i.e. a decrease in f_oF2 compared to undisturbed conditions,

which is associated with a decrease in the F2-layer maximum electron density. In the 80°–110° E sector (zone of the East Siberian Continental Magnetic Anomaly) symmetrical to the geomagnetic pole located in the Western Hemisphere, the level of GMF variations is always lower than in neighboring longitude regions. Accordingly, over Eurasia at ~80°–110° longitudes there is a region of ionization that is higher than that at neighboring longitudes in the F2-region (red oval in Figure 3, *b*). At these longitudes, ionospheric ionization is earlier restored to the undisturbed level after geomagnetic storms [Shpynev et al., 2018; Chernigovskaya et al., 2019; Chernigovskaya et al., 2021a].

ANALYSIS OF MEASUREMENTS OF IONOSPHERIC IONIZATION IN THE NORTHERN HEMISPHERE

For comparison, Figure 3 plots the longitude-time variations characterizing the ionospheric ionization over Eurasia in 50°–60° N during a series of storms in March 2012 as obtained by mid-latitude chains of GPS/GLONASS dual-frequency receivers (*a*) and ionosondes (*b*). Vertical dashed lines show SSCs of the

March 2012 magnetic storms caused by the impact of interplanetary shock waves on Earth's magnetosphere. Variations in ionospheric parameters at heights of the F2-layer ionization maximum in midlatitudes of Eurasia has been analyzed in detail by Chernigovskaya et al. [2022a, b], using data from a chain of seven ionosondes during increased geomagnetic activity in March 2012.

During a long geomagnetically disturbed period including a sequence of intense (strong or moderate) magnetic storms, global changes occur in the GMF structure (compression of the magnetosphere under the impact of an interplanetary shock wave of the disturbed solar wind; reconnection of interplanetary and geomagnetic field lines; fluctuations in the size of the magnetosphere when interacting with an enhanced solar plasma stream; westward ring current amplification due to penetration of new particles into the magnetosphere and plasma acceleration; generation of a field, opposite to the geomagnetic one, due to the auroral electrojet, hence a decrease in the GMF *H* component). Both radiophysical methods in use will therefore show similar variations, which is confirmed by the results presented in Figure 3. We can conclude that the distributions in panels *a*, *b* qualitatively agree quite well. That is why further in our research we can utilize the data on TEC variations to describe the global longitude ionospheric irregularities in regions where there are no ionosondes in the latitude range of interest as an addition to the data set from ground-based ionosonde measurements.

TEC variations obtained from the mid-latitude GPS/GLONASS receiver chain data (see Figure 3, *a*) confirm the complex physical mechanism of the long magnetically disturbed period in March 2012 with a change-over from the ionospheric storm positive phase (S1, S2, March 7–10, 2012) to the negative one (S3, S4, March 12 and 15, 2012) for various longitude ranges of the mid-latitude region in the Eastern Hemisphere. In TEC variations, the main characteristic features of the period are most pronounced: 1) the effect of the development of a positive ionospheric storm over the entire mid-latitude territory of Eurasia (panel *a*) during the main and recovery phases of the March 7, 2012 moderate magnetic storm (S1 in panel *b*); 2) intense positive disturbance in the ionosphere over a vast territory of

Siberia and the Far East (panel *a*) during the main and recovery phases of the March 9, 2012 strong magnetic storm (S2 in panel *c*).

The chain of mid-latitude ionosondes covers only Eurasia; unfortunately, there are no ionosondes in the Western Hemisphere in midlatitudes in the range 50°–60° N of the North American continent [https://giro.uml.edu/ionoweb] (see Figure 1, *b*). Analysis of longitude distributions of GMF variations shows, however, that in the North American sector there may be regions of significant variations in ionospheric parameters associated with zones of enhanced penetration of geomagnetic disturbances into midlatitudes (see Figure 2, *a*). For this reason, we have used data from mid- and high-latitude chains of GPS/GLONASS dual-frequency phase receivers to complete the study of longitude variations in the mid- and high-latitude ionosphere of the Northern Hemisphere during a series of March 2012 magnetic storms related to GMF variations (see Figure 1, *a*). The TEC data covering not only the mainland of Eurasia and North America, but also oceanic islands allowed us to examine a much larger spatial scale of the development of the ionospheric disturbance associated with the evolution of the long geomagnetic disturbance.

Take a closer look at the global spatio-temporal TEC variations (Figure 4) for middle (*a*) and high (*b*) latitudes of the Northern Hemisphere. At increasing magnetic activity, ionization variability is lower in high latitudes than in middle latitudes. This effect was also observed in [Araujo-Pradere et al., 2005].

It can be noted from the maps of longitude-time TEC variations (panels *a*, *b*) that the longitude differences in TEC variations between the Eastern (positive longitude) and Western (negative longitude) hemispheres during the series of March 2012 magnetic storms under study show up most vividly in middle and high latitudes.

First of all, the positive ionospheric storm effect that was observed during the March 7–10, 2012 magnetic storms (S1, S2) in data from mid-latitude ionosondes over Europe, Siberia, and the Far East [Chernigovskaya et al., 2022a, b], and by the authors of [Habarulema et al., 2015, 2016; Verkhoglyadova et al., 2016; Belehaki et al., 2017; Krypiak-Gregorczyk, 2019] in data from ionosondes and GPS receivers over Western Europe and Africa did not
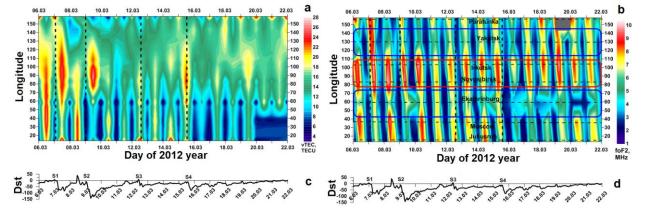

Figure 3. Longitude-time variations in TEC, as obtained by the mid-latitude GPS/GLONASS receiver chain (*a*), and in *f*ₒF2, as derived from the Eurasian mid-latitude ionosonde chain data (*b*) [Chernigovskaya et al., 2022a] in March 2012 (UT). Vertical dashed lines mark SSCs. Variations in the geomagnetic activity index *Dst* (*c*, *d*)
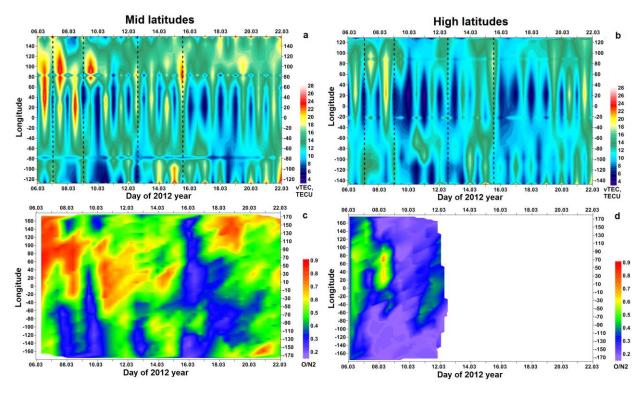
Figure 4. Longitude-time TEC variations as measured by mid- (*a*) and high-latitude (*b*) chains of GPS/GLONASS receivers; longitude-time distributions of [O]/[N$_2$] as measured by TIMED/GUVI for middle (*c*) and high (*d*) latitudes in March 2012 (UT)

reveal itself at all at the longitudes of the Western Hemisphere over North America in measurement data from GPS/GLONASS receivers (panels *a*, *b*). There are low TEC values at the longitudes of the Western Hemisphere during the March 7–10, 2012 storms in both middle (Figure 4, *a*) and high (panel *b*) latitudes.

It is appropriate to recall here that during the March 7–20, 2012 magnetic storms the most significant longitude variations in the GMF components occurred in the midlatitudes of the Western Hemisphere (see Figure 2, *a*). Consequently, at these longitudes, disturbances from the high-latitude ionosphere penetrated to midlatitudes as much as possible. These regions usually exhibit strong negative ionospheric disturbances, i.e. a decrease in f_oF2 compared to undisturbed conditions, which is associated with a decrease in the F2-layer maximum electron density. It is the negative ionospheric storm effect at the longitudes of the Western Hemisphere that is illustrated by panels *a*, *b*.

Bottom panels of Figure 4 show longitude-time distributions of [O]/[N$_2$] in the atmospheric gas column in the thermosphere (ionosphere) above ~100 km for mid-latitude 55°–56° N (*c*) and high-latitude 69°–71° N (*d*) ranges, as measured by the TIMED/GUVI UV spectrograph [Christensen et al., 2003]. The distribution of [O]/[N$_2$] in panel *d* for the high-latitude circle is available only for March 6–12, 2012 probably due to a change in the inclination of the TIMED orbit. Complex electrodynamic processes occurring under conditions of increased geomagnetic activity in polar latitudes lead to a strong decrease in [O]/[N$_2$] in the thermosphere. This physical parameter is a good indicator of negative phases of ionospheric storms [Prölss, Werner, 2002; Laštovička, 2002; Danilov, 2003; Liou et al., 2005; Klimenko et al.,

2011]. After having compared the ionospheric ionization variations at the F2-layer height in the midlatitudes of the Eastern Hemisphere over Eurasia (see Figure 3, *a*, *b*), ionospheric TEC (see Figure 4) of middle (*a*) and high (*b*) latitudes of the Northern Hemisphere with the neutral composition in the same latitudes (*c*, *d*), we can conclude that variations in these parameters correlate very well.

The significant difference in the response of the ionosphere of the Northern Hemisphere at different longitudes, recorded by ionosondes of the Eurasian mid-latitude chain and by mid- and high-latitude chains of GPS/GLONASS receivers during magnetic storms in March 2012, is confirmed by the spatial-temporal distribution of [O]/[N$_2$] as measured by TIMED/GUVI (Figure 4, *c*, *d*). Over Eurasia (longitudes of the Eastern Hemisphere) during SSCs of magnetic storms S1 and S2 on March 7 and 9, 2012, [O]/[N$_2$] was high, as measured by TIMED/GUVI. At the same time there was a large region of low [O]/[N$_2$] over North America (Western Hemisphere longitudes). It is obvious that the Western Hemisphere was dominated by disturbances extending to middle latitudes from the high-latitude ionosphere. Thus, the scenario for a negative ionospheric storm unfolded in contrast to the Eastern Hemisphere that was dominated by the extension of the equatorial ionization anomaly to middle latitudes. This fact is confirmed by measurement data from the mid-latitude chain of INTERMAGNET magnetometers, which showed a significantly lower level of GMF variability in the midlatitudes of the Eastern Hemisphere as compared to the Western Hemisphere (see Figure 2, *a*).

Of particular interest was the response of the mid-latitude ionosphere to the moderate storm S4 (G2 class) (see Figure 3, *c*, *d*), which began on March 15, 2012. During the recovery phase from March 16 to March 18, the storm was accompanied by a CH HSS event, which led to a longer storm recovery phase. According to the data from all mid-latitude ionosondes over Eurasia, the effect of a negative ionospheric storm was manifested (see Figure 3, *b*) during the magnetic storm main and recovery phases [Chernigovskaya et al., 2022a, b]. GPS/GLONASS measurements confirmed the negative ionospheric storm effect (Figure 4) for the middle (*a*) and high (*b*) latitudes of the Northern Hemisphere. On March 16–17, 2012, there was a deep minimum of $[O]/[N_2]$ for the midlatitudes of the Eastern and Western hemispheres (see Figure 4, *c*).

Figure 5, *b* displays a sequence of maps of global spatial distributions of $[O]/[N_2]$ at thermospheric heights above ~100 km according to TIMED/GUVI data for each day of March 6–21, 2012 in the Northern Hemisphere [http://guvitimed.jhuapl.edu/guvi-galleryl3on2]. Day-to-day evolution of these global maps allows us to visually analyze the motion of large-scale regions of lower $[O]/[N_2]$ in the Northern Hemisphere midlatitudes. This analysis makes it possible to once again test the hypothesis that an atmospheric gas wave with lower $[O]/[N_2]$ is formed in the lower thermosphere of polar latitudes during the magnetic storm main phase. After forming in the polar regions of the thermosphere, this wave then extends to the midlatitudes of the Northern Hemisphere and moves westward for several days during the storm recovery phase. Due to the high frequency of collisions between molecular ions and neutrals, such a wave acquires a large scale and momentum and moves over long distances even though the ionospheric source is "switched off" in auroral latitudes [Shpynev et al., 2018; Chernigovskaya et al., 2019, 2022b; Chernigovskaya et al., 2021a]. As emphasized above, $[O]/[N_2]$ is one of the key parameters determining the state of the ionosphere—thermosphere system during ionospheric storms. A decrease in $[O] [N_2]$ in the thermospheric gas causes the electron density to decrease in this region and hence the negative ionospheric storm effect to develop. To trace the relationship between $[O]/[N_2]$ and ionospheric ionization variations, Figure 5, *a* shows a map of longitude-time distribution of TEC derived from the data obtained by the mid-latitude chain of GPS/GLONASS receivers. In the mid-latitude region, as noted above, the ionospheric response to an increase in geomagnetic activity is more pronounced.
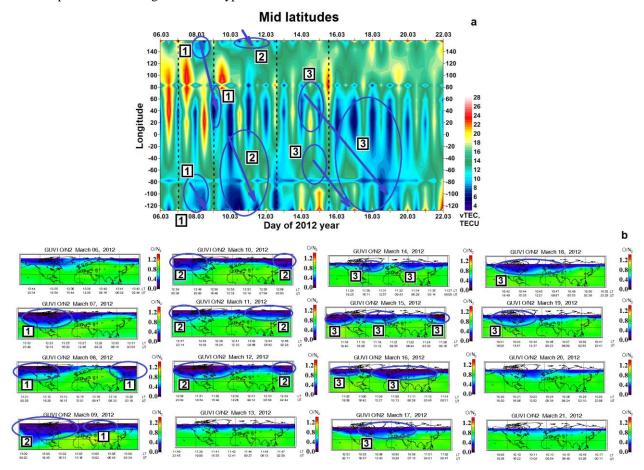

Figure 5. Longitude-time variations in TEC according to data from the mid-latitude chain of GPS/GLONASS receivers (*a*). Maps of global spatial distributions of $[O]/[N_2]$ at thermospheric heights above 100 km as measured by TIMED/GUVI for each day of March 6–21, 2012 in the Northern Hemisphere (*b*). Blue ovals are regions of lower $[O]/[N_2]$, numbered 1, 2, 3. Inclined blue arrows represent the motion of regions with lower TEC (*a*) associated with the spatial movement of a large-scale wave with lower $[O]/[N_2]$ from east to west

The satellite measurement data on [O]/[N$_2$] presented in Figure 5, *b* indicates that a large region of lower [O]/[N$_2$] formed in the Western Hemisphere over North America on March 7, 2012 immediately after SSC of the moderate magnetic storm S1 (oval 1). To this [O]/[N$_2$] decrease corresponds a TEC decrease at longitudes 80°–120° W (oval 1 in Figure 5, *a*). The region of higher [O]/[N$_2$] was detected on March 7, 2012 at longitudes of the Far East and Siberia; on March 8, it shifted westward to the longitudes of Europe. At these longitudes, the positive ionospheric storm effect was observed during the magnetic storm S1 (see Figure 3, *a*, *b*) [Chernigovskaya 2022a, b). On March 8, 2012, region 1 with lower [O]/[N$_2$] shifted westward to the Pacific Ocean and the Far East during the S1 recovery phase. To it corresponds a decrease in TEC at 140°–160° E (oval 1 in the top part of Figure 5, *a*). The ionization decrease on March 8, 2012 is also confirmed by the data from Paratunka and Yakutsk ionosondes (see Figure 3, *b*) [Chernigovskaya 2022a, b]. A negative ionospheric storm developed over the Far East, whereas there was a positive ionospheric storm over the neighboring longitude regions of mid-latitude Eurasia. On the following day, March 9, 2012, region 1 with lower TEC moved westward to the European region.

A strong magnetic storm (S2, class G4) began on March 9, 2012. Disturbances in the polar thermosphere and ionosphere intensified again under these conditions. As a result, [O]/[N$_2$] decreased still further at the heights of the upper atmosphere in polar regions. The region with lower [O]/[N$_2$] extended to middle latitudes up to the low ones in the Western Hemisphere during the S2 main and recovery phases. A more extensive region of lower [O]/[N$_2$] was formed in the Western Hemisphere over midlatitudes of the American continent (region 2), which by March 10, 2012 moved to the Pacific Ocean region, reached 140°–160° E, and was again recorded over the Far East (oval 2 at the top of Figure 5, *a*). The negative ionospheric storm effect was most pronounced in the data from Paratunka and Yakutsk ionosondes (see Figure 3, *b*). The formation of giant region (2) with lower [O]/[N$_2$] at the longitudes of the Western Hemisphere supports the conclusion that the region of more intense penetration of disturbances from high latitudes to middle ones was located in this longitude sector. There was also a zone of maximum GMF variations in this region (see Figure 2, *a*) during the magnetic storms in March 2012 [Chernigovskaya et al., 2022a]. On the following days, March 11–12, 2012 during the S2 recovery phase, the region of lower [O]/[N$_2$] moved over Eurasia from the Eastern Hemisphere to the Western Hemisphere and further to the Pacific Ocean and the coast of the Far East.

During the recovery phase of magnetic storm S3 (G2 class) the weakest in the analyzed period, [O]/[N$_2$] tended to increase in the mid-latitude region at all longitudes on March 13 (see Figure 5, *b*). Accordingly, there were no significant ionization variations (see Figure 5, *a*). Nonetheless, geomagnetic activity in the polar region increased again already on March 14 and with the beginning of moderate magnetic storm S4 (G2 class) on March 15,

2012, which, in addition to CMEs, was accompanied by a CH HSS event from March 16 to March 18. This again led to the formation of a vast wave-like region of lower [O]/[N$_2$] over Europe and eastern North America on March 14, 2012 (region 3). On March 15, 2012, this wave shifted westward to the longitudes of Western Europe, North America, the Pacific Ocean, and the Far East. By March 16, region 3 shifted to Siberia and Europe; on March 16, to the Atlantic Ocean; on March 17–19, to the American continent in the Western Hemisphere.

During the long recovery phase of magnetic storm S4 on March 16–20, 2012, when an extensive wave of lower [O]/[N$_2$] was formed over almost the entire mid-latitude circle, which moved westward (see Figure 5, *b*), there was a negative ionospheric storm effect (see Figure 4, *a*) over all longitudes of the mid-latitude region in the Northern Hemisphere. A significant long-term decrease in ionization was observed over North America at the longitudes of the Western Hemisphere (see Figure 5, *a*) and over Europe in the Eastern Hemisphere (see Figure 3, *b*) almost until March 20, 2012.

Already on March 17, 2012, ionospheric ionization over Siberia and the Far East at 80°–110° E recovered to undisturbed levels earlier than over other regions (see Figure 5, *a* and Figure 3, *b*). This substantiates the conclusions about lower variations of the GMF components in this longitude sector (see Figure 2, *a*) [Shpynev et al., 2018; Chernigovskaya et al., 2019, 2022a, b; Chernigovskaya et al., 2021a].

DISCUSSION OF THE RESULTS OF EXPERIMENTAL DATA ANALYSIS

Physical mechanisms responsible for the ionospheric storms (positive and negative) in March 2012

Ionospheric effects of the long period of geomagnetic disturbances in March 2012 have been analyzed in a number of papers [Habarulema et al., 2015, 2016; Verkhoglyadova et al., 2016; Belehaki et al., 2017; Krypiak-Gregorczyk, 2019], using ionosonde and GPS/GLONASS receiver data. All authors observed the positive ionospheric storm effect over Western Europe and the African continent (in both hemispheres) during the March 7–10, 2012 magnetic storms (S1, S2). The authors consider the extension of the equatorial ionization anomaly to midlatitudes as the main cause of the positive ionospheric storm.

Habarulema et al. [2015, 2016] emphasize, however, that the physical mechanism of this particular geomagnetic disturbance was complex. During the entire disturbed period on March 7–17, 2012, a series of geomagnetic storms S1–S4 occurred [Tsurutani et al., 2014]. That is why the scenario for the ionospheric response to the geomagnetic disturbance changed after March 10, 2012 (S3–S4). Some stations of the meridian chains of GPS receivers and ionosondes, analyzed by the authors, detected the negative ionospheric storm effect. This may be interpreted as dissipation of the su-

perfountain energy when the equatorial anomaly structure expands to the pole. According to the authors, there is a superposition of the effect of increasing electron density due to the extension of the equatorial ionization anomaly to the background ionosphere and the effect of a change in the composition of the auroral thermosphere, which is responsible for the development of a negative ionospheric storm. In such cases, there may be a change-over from the ionospheric storm positive phase to the negative one.

The long-term event of increased heliogeomagnetic activity in March 2012 was extremely effective in terms of its possible impact not only on the ionosphere, but also on the atmosphere. Anagnostopoulos et al. [2022] claim that March 2012 saw two extreme phenomena in near-Earth space: firstly, a historically extreme heat wave in the USA and Canada and, secondly, an increase in the intensity of solar energetic particles, SEPs, (protons, ions, and electrons). We have mentioned in Section "Analysis of heliogeomagnetic conditions and GMF variations" that a series of CME-related large solar flares, as well as a CH HSS event, occurred during the time period we analyze. During the SEP event, a proton spectrum extending to very high (>0.5 GeV) energies was recorded. The CME-related SEP event in March 2012 was accompanied by unusually strong electron precipitation in the high-latitude ionosphere [Anagnostopoulos et al., 2022]. We can recognize the manifestation of this event by the negative ionospheric storm effect over North America from GPS/GLONASS data (see Figure 4, *a*, *b*), as well as by the large region of low $[O]/[N_2]$, as measured by TIMED/GUVI over North America (see Figure 4, *c*, *d*). It is obvious that the Western Hemisphere was dominated by disturbances developing during periods of increased heliogeomagnetic activity in the high-latitude ionosphere.

Anagnostopoulos et al. [2022] note that March 2012 in North America was the warmest on record since March 1910. In fact, it was a meteorological March madness due to a sharp increase in temperature from –2 to 28° C by 30°. Daily average temperatures exceeded the norm by 15–20 °C. The authors attribute this temperature anomaly in March 2012 to unusually complex interplanetary conditions caused by solar activity. In addition to high-energy solar protons (>0.5 GeV), which seem to play a major role, high-speed solar wind streams (CH HSS) and strong precipitation of magnetospheric electrons may have contributed to the generation of large-scale warm air flows (waves) from the Gulf of Mexico to the northeastern United States and Canada. The presence and motion of large-scale neutral atmospheric gas structures during the March 2012 geomagnetic event we analyze furnish convincing proof of the sequence of maps of global spatial distributions of $[O]/[N_2]$, as measured by TIMED/GUVI in the Northern Hemisphere in March 2012 (see Figure 5, *b*).

Comparing radiophysical methods of ionospheric ionization analysis

The radiophysical measurement methods we adopt complement and enrich each other. The vertical sounding method allows us to analyze in detail spatio-temporal features of variations in ionospheric parameters at the height of the ionization maximum in the F2 layer and the underlying layers of the ionosphere during ionospheric disturbances. The method for remote sensing of the ionosphere by GPS/GLONASS satellite signals, which provides integral characteristics of the ionosphere, can effectively investigate global features of ionospheric irregularities.

Earlier, we have observed a fairly good qualitative agreement between space-time distributions of ionospheric ionization, as measured by ground-based vertical sounding and by chains of GPS/GLONASS double-frequency phase receivers (see Figure 3, *a*, *b*). We have received similar results in our previous studies of extreme magnetic storms in March and June 2015 [Chernigovskaya et al., 2020; Chernigovskaya et al., 2021a]. This once again proves the well-established fact that the ionospheric region located in the vicinity of the main ionization maximum, i.e. the F2 layer, makes a major contribution to TEC ([Afraimovich, Perevalova, 2006] and references therein).

Yet, there are also obvious differences whose causes need to be discussed. To explain the observed differences between the patterns of longitude-time variations in f_oF2 and TEC, we should take into account the significant difference in the physical nature of the ionospheric parameters considered. Integral TEC includes the contribution of the region above the ionization maximum (the outer ionosphere and plasmasphere) [Krinberg, Tashchilin, 1984], where ground-based ionosondes do not work.

The question about the contribution of the outer ionosphere and the plasmasphere to the global distribution of TEC has not been answered yet, although its solution is very important. Almost all the works attempting to study the contribution of the outer ionosphere and the plasmasphere to TEC were based on numerical simulation with various models. At the same time, most studies were carried out just for a limited range of longitudes and latitudes, and only a small number of studies attempted to solve this problem on a global scale [Kosov et al., 2018].

Quite diverse results have been obtained depending on the type of model and geomagnetic conditions. All researchers have noted the presence of seasonal, diurnal, as well as latitudinal variations in the contribution of the outer ionosphere and the plasmasphere to TEC. For example, Bilitza [2009] has found that about 80 % of TEC in the ionosphere occurs in the part located above the F-layer peak known as the upper (outer) ionosphere. Yizengaw et al. [2008] argue that the relative contribution of the plasmaspheric electron content depending on latitude has a diurnal variation, i.e. it is minimum (~10 %) during the day and maximum (to 60 %) at night. The contribution is also maximum in the equatorial region, where the GPS ray path travels a long distance through the plasmasphere compared to its length in middle and high latitudes.

Joint analysis of data from the Irkutsk Incoherent Scatter Radar and GPS TEC data [Shpynev, Khabituev, 2014] has revealed that the contribution of the plasmasphere electron density to TEC can be 30–50 % in summer

and equinoctial seasons. In winter in the absence of ionization sources in the lower ionosphere, the total ionization of the plasmasphere is low and the entire F2 layer is formed within a small range of heights 200–400 km.

Klimenko et al. [2015a] show that the mid-latitude ionosphere during the storm main phase is more variable than the plasmasphere and makes a major contribution to TEC perturbations. At the same time, spatial regions are formed in the middle and equatorial latitudes, in which the contribution of the plasmasphere to TEC increases by 20–25 %. Klimenko et al. [2015b], using results of model calculations and ground-based and GPS and COSMIC satellite observations, show that the contribution of the plasmasphere to TEC (to 85 %) is maximum near the equator at night. The daily contribution of the plasmasphere to TEC does not exceed ~40 %, which agrees with the results of previous studies [Balan et al., 2002].

Yasyukevich et al. [2020] indicate that the contribution of the plasmasphere to TEC depends on local time and season. During the daytime, the plasmaspheric electron content (PEC) is 25–30 % of TEC and is minimum around noon. At night, the contribution of the plasmasphere increases significantly: on average, it is about half of TEC, and in some periods it is as high as 70 %. At high latitudes, the contribution of the nightside plasmasphere is greater than at midlatitudes. The PEC/TEC ratio begins to increase after sunset and peaks before sunrise. It does not change with an increase in solar activity. It has been found that the IRI-Plas model significantly underestimates the level of the plasmasphere contribution to TEC, especially at night.

Prol et al. [2021], using a new tomographic reconstruction method to estimate the electron density from data on TEC along METOP (METeorological OPerational) satellites, have shown that the plasmaspheric TEC contribution to integral TEC can change by 10–60 % during geomagnetic storms, and in the storm recovery phase it tends to decrease.

Habarulema et al. [2021] have first statistically determined the contribution of the upper ionosphere to GPS TEC from COSMIC radio-eclipsing data and have revealed that it accounts for ~50 % of TEC at low solar activity. The analysis has demonstrated that determining the contribution of electron content at different heights is important for understanding the mechanisms of ionospheric storms during space weather phenomena, especially geomagnetic storms.

Review of even a small number of the above-mentioned studies on this topic suggests that the question about the relative contribution of the inner and outer ionosphere with the plasmasphere to TEC is still far from a final solution and is very relevant.

CONCLUSIONS

The study of variations in ionospheric parameters at midlatitudes of the Northern Hemisphere from GPS/GLONASS receiver, ionosonde, and INTERMAGNET magnetometer data during a series of geomagnetic storms in March 2012 supports the previously formulated conclusions [Shpynev et al., 2018; Cherni-

govskaya et al., 2019, 2020, 2021b; Chernigovskaya et al., 2021a] that 1) the structure of the magnetospheric-ionospheric current system during magnetic storms depends on spatial anomalies in the main geomagnetic field, manifested in variations of GMF and ionospheric parameters; 2) low ionization values during the long recovery phase of the storm (2–4 days after the main phase) may be due to westward propagation of an atmospheric wave of neutral gas with low $[O]/[N_2]$ over the mid-latitude region over long distances even through the ionospheric source is "switched off" in auroral latitudes.

The comprehensive study allows us to draw the following conclusions.

We have confirmed the results that the structure of the longitude variability in the GMF components under quiet and disturbed conditions is irregular due to the mismatch between the North geographic and geomagnetic poles (UT effect), as well as due to the presence of anomalies of various spatial scales in the main geomagnetic field.

During a magnetic storm, variations in main GMF become significant. They can play an essential role in forming longitudinal irregularities of the ionosphere, especially during the storm recovery phase.

We have emphasized the complex physical mechanism of the magnetically disturbed period with changeover from the ionospheric storm positive phase to the negative one during the March 7–10, 2012 magnetic storms for different longitude regions of the mid-latitude region in the Northern Hemisphere. The change in the ionospheric storm effects during the period under study might have been linked to the superposition in the mid-latitude region of competing processes affecting ionospheric ionization, whose sources are located in the auroral ionosphere (a series of intense solar activity events that led to geomagnetic storms on March 7, 9, 12, 15, 2012 and to a significant disturbance of the high-latitude atmosphere and ionosphere), as well as in the equatorial ionosphere (the superfountain effect at equatorial latitudes on March 7–10, 2012).

We have observed significant differences in the ionospheric response in the Eastern and Western hemispheres to a long geomagnetic disturbance in March 2012.

At the Western Hemisphere longitudes, there was an effect of lower ionospheric ionization according to the TEC data obtained during a series of magnetic storms in March 2012. This ionospheric response was induced by the formation of vast regions of lower $[O]/[N_2]$ over the mid-latitude region of the Western Hemisphere in the zone of maximum penetration of geomagnetic disturbances from high to middle latitudes. This is confirmed by the observation of increased variations of GMF components in the Western Hemisphere, as measured at the mid-latitude chain of INTERMAGNET magnetometers.

The vast regions of lower $[O]/[N_2]$ were formed in the Western Hemisphere over North America immediately after SSC of the March 7, 2012 moderate magnetic storm S1 and SSC of the March 9, 2012 strong magnetic storm S2 as large-scale thermospheric waves of molecular gas

propagating westward for several days.

Over mid-latitude Eurasia at ~80°–110° longitudes, the ionosphere recovered earlier after the geomagnetic disturbances due to lower GMF variations in this longitude sector.

REFERENCES

Afraimovich E.L. Perevalova N.P. *GPS-monitoring verkhnei atmosfery Zemli (GPS-monitoring of the Earth upper atmosphere)*. Irkutsk: GU NTs VSNTs SO RAMN, 2006, pp. 90–94. (In Russian).

Anagnostopoulos G.C., Menesidou S.-A.I., Efthymiadis D.A. The March 2012 heat wave in Northeast America as a possible effect of strong solar activity and unusual space plasma interactions. *Atmosphere*. 2022, vol. 13, iss. 6, p. 926. DOI: 10.3390/atmos13060926.

Araujo-Pradere E.A., Fuller-Rowell T.J., Codrescu M.V., Bilitza D. Characteristics of the ionospheric variability as a function of season, latitude, local time, and geomagnetic activity. *Radio Sci*. 2005, vol. 40, RS5009. DOI: 10.1029/2004RS003179.

Astafyeva E.I. Dayside ionospheric uplift during strong geomagnetic storms as detected by the CHAMP, SAC-C, TOPEX and Jason-1 satellites. *Adv. Space Res*. 2009, vol. 43, pp. 1749–1756. DOI: 10.1016/j.asr.2008.09.036.

Balan N., Otsuka Y., Tsugawa T., Miyazak, S., Ogawa T., Shiokawa K. Plasmaspheric electron content in the GPS ray paths over Japan under magnetically quiet conditions at high solar activity. *Earth, Planets and Space*. 2002, vol. 54, pp. 71–79. DOI: 10.1186/BF03352423.

Belehaki A., Kutiev I., Marinov P., Tsagouri I, Koutroumbas K., Elias P. Ionospheric electron density perturbations during the 7–10 March 2012 geomagnetic storm period. *Adv. Space Res*. 2017, vol. 59, pp. 1041–1056. DOI: 10.1016/j.asr.2016.11.031.

Bilitza D. Evaluation of the IRI-2007 model options for the topside electron density. *Adv. Space Res*. 2009, vol. 44, no. 6, pp. 701–706. DOI: 10.1016/j.asr.2009.04.036.

Buonsanto M.J. Ionospheric storms — a review. *Space Sci. Rev*. 1999, vol. 88, pp. 563–601.

Burešová D., Laštovička J., de Franceschi G. Manifestation of Strong Geomagnetic Storms in the Ionosphere above Europe / In: *Lilensten J. (ed.), Space Weather Springer*. 2007, pp. 185–202.

Chernigovskaya M.A., Shpynev B.G., Khabituev D.S., Ratovskii K.G., Belinskaya A.Yu., Stepanov A.E., et al. Longitudinal variations of geomagnetic and ionospheric parameters during severe magnetic storms in 2015. *Sovremennye problemy distantsionnogo zondirovaniya Zemli iz kosmosa*. 2019, vol. 16, no. 5, pp. 336–347. DOI: 10.21046/2070-7401-2019-16-5-336-347. (In Russian).

Chernigovskaya M.A., Shpynev B.G., Yasyukevich A.S., Khabituev D.S. Ionospheric longitudinal variability in the Northern Hemisphere during magnetic storm from the ionosonde and GPS/GLONASS data. *Sovremennye problemy distantsionnogo zondirovaniya Zemli iz kosmosa*, 2020, vol. 17, no. 4, pp. 269–281. DOI: 10.21046/2070-7401-2020-17-4-269-281. (In Russian).

Chernigovskaya M.A., Shpynev B.G., Yasyukevich A.S., Khabituev D.S., Ratovsky K.G., Belinskaya A.Yu., et al. Longitudinal variations of geomagnetic and ionospheric parameters in the Northern Hemisphere during magnetic storms according to multi-instrument observations. *Adv. Space Res*. 2021a, vol. 67, no. 2, pp. 762–776. DOI: 10.1016/j.asr.2020.10.028.

Chernigovskaya M.A., Shpynev B.G., Yasyukevich A.S., Khabituev D.S., Ratovskii K.G., Belinskaya A.Yu., et al. Longitudinal variations in the response of the mid-latitude ionosphere of the Northern Hemisphere to the October 2016 geomagnetic storm using multi-instrumental observations. *Sovremennye problemy distantsionnogo zondirovaniya Zemli iz kosmosa*. 2021b, vol. 18, no. 5, pp. 305–317. DOI: 10.21046/2070-7401-2021-18-5-305-317. (In Russian).

Chernigovskaya M.A., Shpynev B.G., Khabituev D.S., Ratovsky K.G., Belinskaya A.Yu., Stepanov A.E., et al. Studying the response of the mid-latitude ionosphere of the Northern Hemisphere to magnetic storms in March 2012. *Solar-Terr. Phys*. 2022a, vol. 8, iss. 4, pp. 44–54. DOI: 10.12737/stp-84202204.

Chernigovskaya M.A., Shpynev B.G., Yasyukevich A.S., Khabituev D.S. Response of the ionosphere – thermosphere system over the midlatitude region of Eurasia to geomagnetic storms in March 2012. *Sovremennye problemy distantsionnogo zondirovaniya Zemli iz kosmosa*. 2022b, vol. 19, no. 5, pp. 303–315. DOI: 10.21046/2070-7401-2022-19-5-303-315. (In Russian).

Christensen A.B., Paxton L.J., Avery S., Craven J., Crowley G., Humm D.C., et al. Initial observations with the Global Ultraviolet Imager (GUVI) on the NASA TIMED satellite mission. *J. Geophys. Res*. 2003, vol. 108, no. A12, p. 1451. DOI: 10.1029/2003JA009918.

Danilov A.D. Long-term trends of f_oF2 independent on geomagnetic activity. *Ann. Geophys*. 2003, vol. 21, no. 5, pp. 1167–1176.

Danilov A.D. Response of region F to geomagnetic disturbances (review). *Heliogeophysical research*. 2013, no. 5, pp. 1–33. (In Russian).

Dudok de Wit T., Watermann J. Solar forcing of the terrestrial atmosphere. *Comptes Rendus Geoscience*. 2009, vol. 342, no. 4-5, pp. 259–272. DOI: 10.1016/j.crte.2009.06.001.

Habarulema J.B., Katamzi Z.T., Yizengaw E. First observations of poleward large-scale traveling ionospheric disturbances over the African sector during geomagnetic storm conditions. *J. Geophys. Res. Space Physics*. 2015, vol. 120, pp. 6914–6929. DOI: 10.1002/2015JA021066.

Habarulema J.B., Katamzi Z.T., Yizengaw E., Yamazaki Y., Seemala G. Simultaneous storm time equatorward and poleward large-scale TIDs on a global scale. *Geophys. Res. Lett*. 2016, vol. 43, pp. 6678–6686. DOI: 10.1002/2016GL069740.

Habarulema J.B., Okoh D, Bergeot N., Burešová D., Matamba T., Tshisaphungo M., et al. Interhemispheric comparison of the ionosphere and plasmasphere total electron content using GPS, radio occultation and ionosonde observations. *Adv. Space Res*. 2021, vol. 68, iss. 6, pp. 2339–2353. DOI: 10.1016/j.asr.2021.05.004.

Huang C.M. Disturbance dynamo electric fields in response to geomagnetic storms occurring at different universal times. *J. Geophys. Res.: Space Phys*. 2013, vol. 118, pp. 496–501. DOI: 10.1029/2012JA018118.

Klimenko M.V., Klimenko V.V, Ratovsky K.G., Goncharenko L.P., Fagundes R.R., de Jesus R., de Abreu A.J., Vesnin A.M. Numerical modeling of ionospheric effects in the middle- and low-latitude F region during geomagnetic storm sequence of 9–14 September 2005. *Radio Sci*. 2011, RS0D03. DOI: 10.1029/2010RS004590.

Klimenko M.V., Klimenko V.V., Bessarab F.S., Zakharenkova I.E., Kotova D.S., Nosikov I.A., et al. Influence of geomagnetic storms of September 26–30, 2011, on the ionosphere and radiowave propagation. I. Ionospheric effects. *Geomagnetism and Aeronomy*. 2015a, vol. 55, no. 6, pp. 744–762. DOI: 10.1134/S0016793215050072.

Klimenko M.V., Klimenko V.V., Zakharenkova I.E., Cherniak Iu.V. The global morphology of the plasmaspheric electron content during Northern winter 2009 based on

GPS/COSMIC observation and GSM TIP model results. *Adv. Space Res*. 2015b, vol. 55, no. 8, pp. 2077–2085. DOI: 10.1016/j.asr.2014.06.027.

Kosov A.S., Chernyshov A.A., Mogilevsky M.M., Chugunin D.V., Korogod V.V., Munitsyn V.A., Dolgonosov M.S., Skulachev D.P. Space Experiment on Measuring Ionospheric Signal Delay RWIS (Radio Waves Ionosphere Sensing). *Issledovanie Zemli iz kosmosa*. 2018, no. 6, pp. 13–23. DOI: 10.31857/S020596140003364-1. (In Russian).

Krinberg I.A., Tashchilin A.V. Ionosfera i plazmosfera. M.: Nauka Pabl., 1984, 129 p. (In Russian).

Krypiak-Gregorczyk A. Ionosphere response to three extreme events occurring near spring equinox in 2012, 2013 and 2015, observed by regional GNSS-TEC model. *J. Geodesy*. 2019, vol. 93, pp. 931–951. DOI: 10.1007/s00190-018-1216-1.

Laštovička J. Monitoring and forecasting of ionospheric space weather effects of geomagnetic storms. *J. Atmos. Solar-Terr. Phys*. 2002, vol. 64, pp. 697–705. DOI: 10.1016/S1364-6826(02)00031-7.

Liou K., Newell P.T., Anderson B.J., Zanetti L., Meng C.-I. Neutral composition effects on ionospheric storms at middle and low latitudes. *J. Geophys. Res*. 2005, vol. 110, p. A05309. DOI: 10.1029/2004JA010840.

Loewe C.A., Prölss G.W. Classification and mean behavior of magnetic storms. *J. Geophys. Res*. 1997, vol. 102, no. A7, pp. 14,209–14,213.

Matsushita S. A study of the morphology of ionospheric storms. *J. Geophys. Res*. 1959, vol. 64, no. 3, pp. 305–321. DOI: 10.1029/JZ064i003p00305.

Mayr H.G., Volland H. Magnetic storm effects in the neutral composition. *Planet. Space Sci*. 1972, vol. 20, p. 379.

Mendillo M. Storms in the ionosphere: Patterns and processes for total electron content. *Rev. Geophys*. 2006, vol. 44, RG4001. DOI: 10.1029/2005RG000193.

Polyakov V.M., Shchepkin L.A., Kazimirovsky E.S., Kokourov V.D. *Ionosfernye processy* [Ionospheric processes]. Novosibirsk: Nauka Pabl., 1968, 535 p. (In Russian).

Prol F.S., Hoque M.M., Ferreira A.A. Plasmasphere and topside ionosphere reconstruction using METOP satellite data during geomagnetic storms. *J. Space Weather Space Clim*. 2021, vol. 11, no. 5. DOI: 10.1051/swsc/2020076.

Prölss G.W. Ionospheric F-region storms. In: Volland H. (ed.), *Handbook of atmospheric electrodynamics*. CRC Press, Boca Raton. 1995, vol. 2, ch. 8, pp. 195–248.

Prölss G.W., Werner S. Vibrationally excited nitrogen and oxygen and the origin of negative ionospheric storms. *J. Geophys. Res*. 2002, vol. 107, no. A2, p. 1016. DOI: 10.1029/2001JA900126.

Rishbeth H. How the thermospheric circulation affects the ionospheric F2-layer. *J. Atmos. Solar-Terr. Phys*. 1998, vol. 60, pp. 1385–1402.

Seaton M.J. A possible explanation of the drop in F-region critical densities accompanying major ionospheric storms. *J. Atmos. Terr. Phys*. 1956, vol. 8, p. 122.

Shpynev B.G., Khabituev D.S. Estimation of the plasmasphere electron density and O+/H+ transition height Irkutsk incoherent scatter data and GPS total electron content. *J. Atmos. Solar-Terr. Phys*. 2014, vol. 119, pp. 223–228. DOI: 10.1016/j.jastp.2014. 01.007.

Shpynev B.G., Zolotukhina N.A., Polekh N.M., Ratovsky K.G., Chernigovskaya M.A., Belinskaya A.Yu.,

et al. The ionosphere response to severe geomagnetic storm in March 2015 on the base of the data from Eurasian high-middle latitudes ionosonde chain. *J. Atmos. Solar-Terr. Phys*. 2018, vol. 180, pp. 93–105. DOI: 10.1016/j.jastp.2017.10.014.

Tsurutani B., Mannucci A., Iijima B., Abdu M.A., Sobral J.H.A., Gonzalez W., et al. Global dayside ionospheric uplift and enhancement associated with interplanetary electric fields. *J. Geophys. Res*. 2004, vol. 109, A08302. DOI: 10.1029/2003JA010342.

Tsurutani B., Echer E., Shibata K., Verkhoglyadova O., Mannucci A., Gonzalez W., et al. The interplanetary causes of geomagnetic activity during the 7–17 March 2012 interval: a CAWSES II overview. *J. Space Weather Space Clim*. 2014, vol. 4, no. A02. DOI: 10.1051/swsc/2013056.

Verkhoglyadova O.P., Tsurutani B.T., Mannucci A.J., Mlynczak M.G., Hunt L.A., Paxton L.J., Komjathy A. Solar wind driving of ionosphere-thermosphere responses in three storms near St. Patrick's Day in 2012, 2013, and 2015. *J. Geophys. Res.: Space Phys*. 2016, vol. 121, pp. 8900–8923. DOI: 10.1002/2016JA022883.

Yasyukevich A.S., Yasyukevich Yu.V., Klimenko M.V., Vesnin A.M. Plasmasphere Contribution to Total Electron Content at High and Middle Latitudes. *Proc. URSI GASS 2020*, Rome, Italy, 29 Aug – 5 Sep 2020. PID6354063. https://www.ursi.org/proceedings/procGA20/papers/PID6354063.pdf.

Yasyukevich Yu.V., Mylnikova A.A., Polyakova A.S. Estimating the total electron content absolute value from the GPS/GLONASS data. *Res. Phys*. 2015, vol. 5, pp. 32–33. DOI: 10.1016/j.rinp.2014.12.006.

Yizengaw E., Moldwin M.B., Galvan D., Iijima B.A., Komjathy A., Mannucci A.J. Global plasmaspheric TEC and its relative contribution to GPS TEC. *J. Atmos. Solar-Terr. Phys*. 2008, vol. 70, pp. 1541–1548. DOI: 10.1016/j.jastp.2008.04.022.

URL: http://guvitimed.jhuapl.edu/guvi-galleryl3on2 (accessed March 15, 2023).

URL: http://www.intermagnet.org (accessed February 20, 2023).

URL: http://wdc.kugi.kyoto-u.ac.jp (accessed February 2, 2023).

URL: https://www.swpc.noaa.gov/noaa-scales-explanation (accessed June 2, 2023).

URL: https://giro.uml.edu/ionoweb (accessed June 2, 2023).
URL: http://ckp-rf.ru/ckp/3056/ (accessed June 2, 2023).